Supporting information (SI):

Modification of In_2O_3 by electronic promoters to regulate electron transfer behavior of CO_2/H_2O adsorption and the selectivity of photocatalytic CO_2 reduction

Hong Wang[a,b], Zhongming Wang[a,b], Mingquan Xiao[a,b], Zizhong Zhang[a,b], Xianzhi Fu[a,b]*, Wenxin Dai[a,b]*

[a] Research Institute of Photocatalysis, State Key Laboratory of Photocatalysis on Energy and Environment, Fuzhou University, Fuzhou, 350108, China

[b] Qingyuan Innovation Laboratory, Quanzhou, 362801, China

*Corresponding author: Wenxin Dai & Xianzhi Fu

Tel & Fax: +86-0591-22865893

E-mail: daiwenxin@fzu.edu.cn & xzfu@fzu.edu.cn

Materials and methods:

The sensor sample was synthesised via drop-coating method

A commerci alumina sheet (1.5 cm × 1 cm) with a comb-like gold electrode on one side surface was used as the substrate for sensors. A 50 μL suspension (30 mg of above In_2O_3(B), F-In_2O_3(B) and NH_2-In_2O_3(B) samples was dispersed into a 1 mL ethanediol solvent) was dropped onto the surface of the comb-like gold electrode. Then, this substrate coated with samples suspension was dried at 80 ^oC for 2 h. In_2O_3(B), F-In_2O_3(B) and NH_2-In_2O_3(B) sensor samples were obtained.

Characterization

The phase and crystal structure of samples were characterized by X-ray diffraction (XRD, D8 Advance, Brucker, Germany) having Cu Kα radiation. Powder X-ray diffraction analysis was carried out in the 2θ range 20°-60°. The accelerating voltage was 40 kV and the current was 40 mA. Zeta potentials (ξ) measurements of the samples were determined by dynamic light scattering analysis (Zeta sizer 3000HSA) at room temperature. Electron paramagnetic resonance (EPR) spectra were recorded on a Bruker A300 spectrometer operating at X-band microwave frequency (9.84 GHz). Transmission electron microscopy (TEM) investigation together with an electron-diffraction image was carried out on a JEOL JEM-2010 EX with field emission gun at 200 kV. The electrochemical analysis was carried out in a conventional three-electrode cell using a Pt plate and an Ag/AgCl electrode as the counter electrode and reference electrode through electrochemical workstation (AUT302N.V, Metrohm, Switzerland). The steady-state photoluminescence (PL) spectroscopy were used to

probe fluorescence intensity of samples with excitation wavelength of 325 nm through Hitachi F-7000 fluorescence spectrometer (Hitachi, Tokyo, Japan). The static water contact angles were measured at 25 °C using the optical contact angle meter system (DSA25, KRUSS, Germany).

The X-ray photoelectron sepectroscopy (XPS) and ultraviolet photoelectron spectroscopy (UPS) data of samples were collected using a Thermo Nicolet ESCALAB 250 electron spectrometer. The binding energies were corrected for the charge shift using the C1s peak of graphitic carbon (BE = 284.80 eV) as a calibration.

UPS measurements were carried out using the He I photon line (hυ = 21.2 eV) of a He discharge lamp from VSW dosed with 10^{-7} mbar of He. The analyzer was the same as for the XPS measurements, but now working with a pass energy of 5 eV. When the spectra were collected, samples were -5 V biased. The work functions (Φ) and Fermi level (E_{vm}) are calculated with the equation [1]:

$$\Phi = h\nu - (E_{Cutoff} - E_{Fermi}) \quad \text{Equation (S1)}$$

$$\Phi = E_{vm} - E_{fm} \quad \text{Equation (S2)}$$

where Φ, E_{fm}, E_{vm}, hν, E_{cutoff}, and E_{Fermi} are the work functions, Fermi level, vacuum level, the excitation energy (21.22 eV), the cutoff and the Fermi level edge, respectively.

The contact potential difference between the samples and the spectrometer, versus normal hydrogen electrode (NHE) at pH= 7, was estimated using the formula [2, 3]:

$$E_{NHE}/V = \Phi + VB_{max} - 4.44 \quad \text{Equation (S3)}$$

Where E_{NHE}: potential of normal hydrogen electrode, Φ of 3.88 eV: the electron

work function of the spectrometer.

UV-vis diffuse reflectance spectra (UV-vis DRS) of samples were recorded with UV-vis spectrophotometer (Cary-5000, Varian, U.S.A), the spectra were recorded between 300 and 800 nm using $BaSO_4$ as reference. The band gap energy (E_g) of samples determination from the Tauc plot by the following equation [4]:

$$(\alpha h\nu)^n = A \cdot (h\nu - E_g) \quad \text{Equation (S4)}$$

where h is the Planck constant, ν is the photon's frequency, A is a constant, and n factor depends on the nature of the electron transition and is equal to 1/2 or 2 for the direct and indirect transition band gaps, respectively.

Electron transfer behavior of CO_2/H_2O adsorption

The gas sensing properties of In_2O_3(B), F-In_2O_3(B) and NH_2-In_2O_3(B) sensors were conducted in a 100 mL stainless steel chamber with a quartz window. The response of sample sensors to the gas was described by the variation of its impedance. During the testing process, a high purity N_2 was introduced into the chamber as the background atmosphere, and the 10 % CO_2 balanced with the high purity N_2 and humid N_2 (H_2O) were acted as the probe gas. Among them, H_2O was introduced into the chamber using a bubbling system with nitrogen (humid N_2). The total flow rate was maintained at 250 mL · min^{-1}. The resistance of the film sensor was measured via a JF02F gas sensing test system (Kunming GuiYanJinFeng Tech. Corp. Ltd, its main components seen in Fig. S1) and the applied voltage was controlled at 5.0 V. Prior to any measurement, the film sensor sample was maintained at 100 ℃ for one hour in a high purity N_2 to remove the physical adsorption of H_2O and gas

adsorbates.

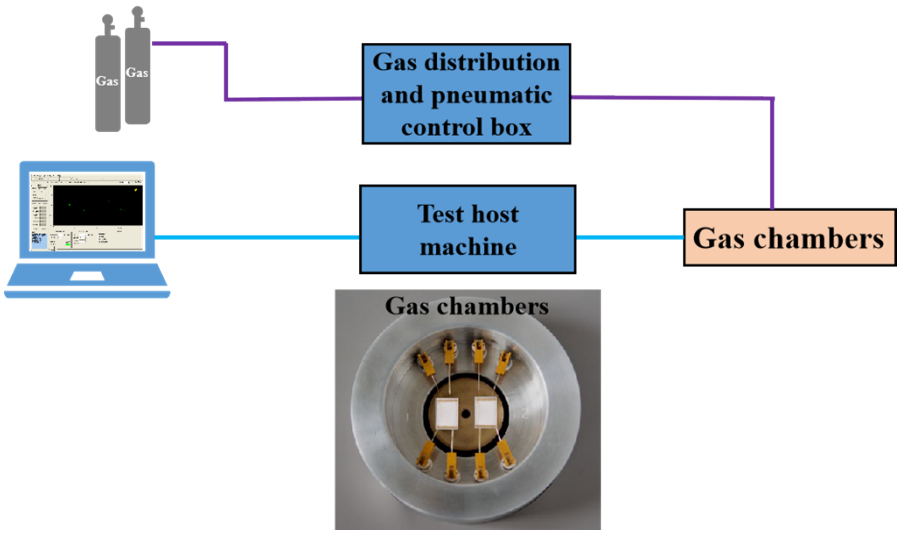

Fig. S1 Schematic diagram of gas sensing test system.

In situ DRIFTS testing

The in-situ diffuse reflectance infrared Fourier transform spectroscopy (in-situ DRIFTS) measurements were conducted using the specially designed in-situ DRIFTS reactor cell tube (its main structure seen in Fig. S2) and smart collector accessory on a Bruker vexter 80v FT-IR Spectrometer with MCT detector. Four UV lamps with a wavelength centered at 365 nm (4 W, Philips TL/05) were used as the radiation source (also as the light source in other experiments in this work, its spectrogram seen in Fig. S4). First, the sample was loaded in an in-situ DRIFTS reactor cell and subjected to evacuation at 100 °C for 1 h in N_2 atmosphere (the total flow rate was maintained at 60 mL· min^{-1}) to remove the physisorbed water/moisture. During this process of the in-situ DRIFTS experiment, the recorded data was within the 4000-1100 cm^{-1} spectral range with a resolution of 8 cm^{-1}. Each spectrum was obtained by averaging 64 scans in order to reduce the signal-to-noise ratios.

After cooled down to room temperature, firstly, UV light was introduced and the sample was collected the spectrum as a collection background under UV radiation for 20 min. Then, the 10% CO_2 (N_2) and humid N_2 (H_2O), as the probe gas was introduced into the system with the total flow rate at 60 mL· min^{-1} for 10min. Cutting down both the inlet and outlet of probe gas, and the datum was collected after 1h dark adsorption and 1h light illumination in N_2 atmosphere to obtain the spectrum of sample.

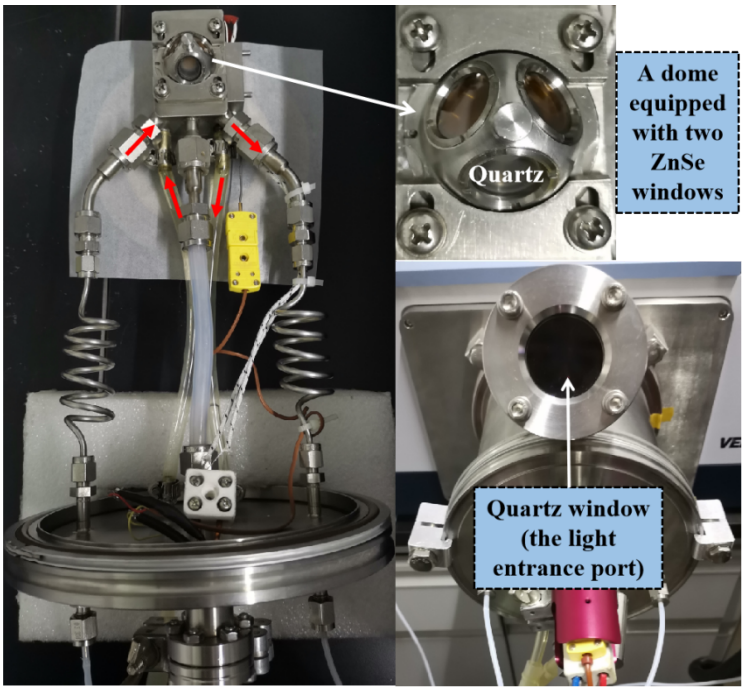

Fig. S2 Main structure of in-situ DRIFTS reactor cell.

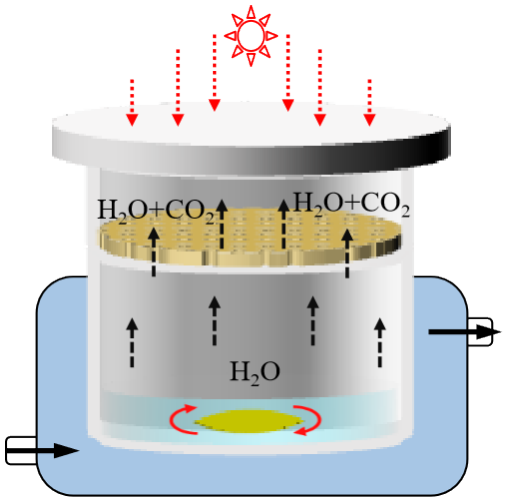

Fig. S3 Schematic diagram of reactor structure.

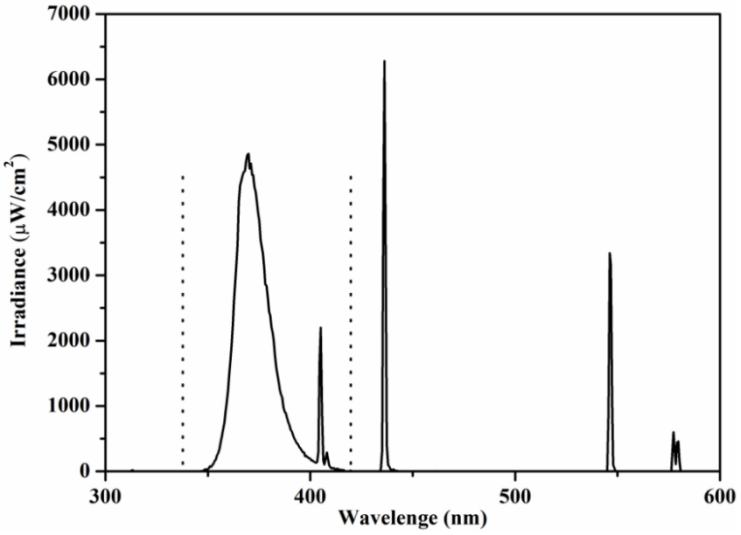

Fig. S4 Spectrogram of the light source used in the experiment.

Results and discussion:

Material characterization

Fig. S5 shows the FTIR spectra of In_2O_3(B) and NH_2-In_2O_3(B) samples. The spectrum of NH_2-In_2O_3(B) exhibits the following bands: The stretching characteristic bands of Si-OH and Si-O in 3425 and 874 cm^{-1} respectively, the asymmetrical and symmetrical stretching -NH in 3265, 3100 and 1631 cm^{-1}, and the bands 798 cm^{-1} can be attributed to regions of angular deformation outside the plane of -NH_2 groups, all of the above infrared peaks were generated from APTES [5], indicating that the surface of In_2O_3(B) was successfully modified with the electronic promoters NH_2^+. In addition, the CH_x (ν_{as} CH_2 and ν_{as} CH_3) (the bands in the range of 2932-2853 cm^{-1}) and C-C (1442 cm^{-1}) species [5, 6] may arise from the isopropyl alcohol.

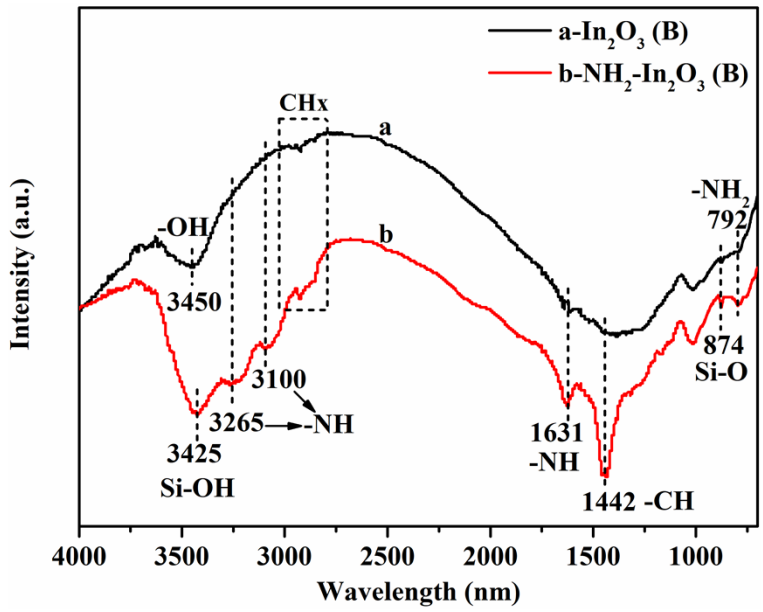

Fig. S5 FTIR spectra of (a) In_2O_3(B) and (b) NH_2-In_2O_3(B) samples.

Photocatalytic performance of CO_2 reduction with H_2O

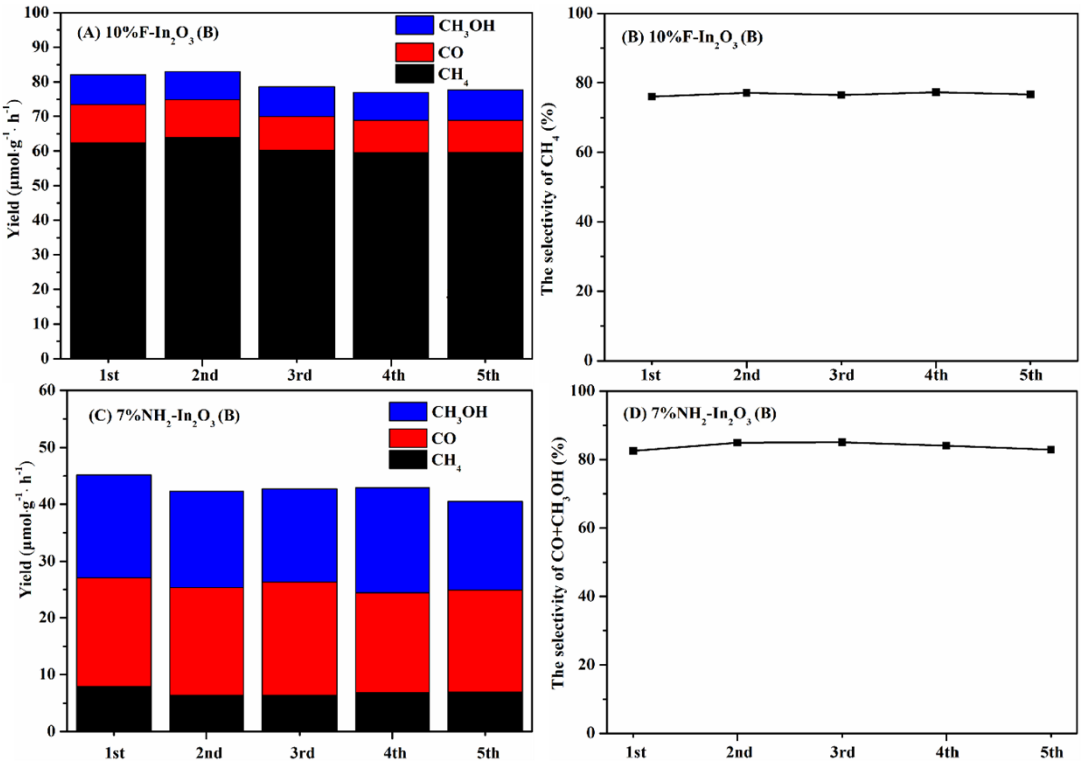

Fig. S6 Stability test of (A, B) 10%F-In_2O_3(B) and (C, D) 7%NH_2-In_2O_3(B) samples.

Results of $^{13}CO_2$+D_2O isotope experiments

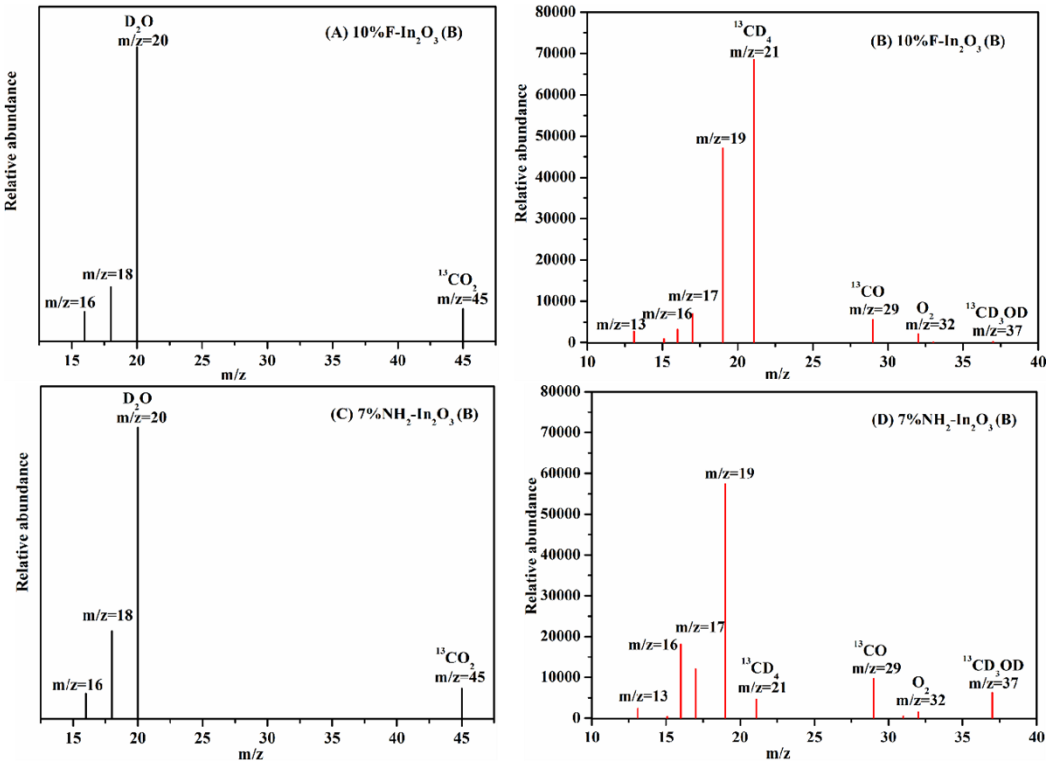

Fig. S7 Mass spectra of $^{13}CO_2$+D_2O isotope experiments over over (A, B) F-In_2O_3 (B) and (C, D) NH_2-In_2O_3 (B) samples.

Photocatalytic CO_2+H_2 reaction performances over different samples

Photocatalytic reduction of CO_2 with H_2 over the material samples were carried out under identical conditions. The reacted gases with high-purity CO_2 (10 mL) and H_2 (30 mL) (CO_2 + H_2 system) were added into the reactor. Subsequently, the reactor was heated to 80 ℃ via a constant-temperature H_2O bath, and the reaction products were detected after UV radiation for 1 h by an gas chromatograph. The activity results under UV radiation were shown in Fig. S8, the overall activity of photocatalytic CO_2 reduction with H_2 over three samples was significantly improved as compared to CO_2+H_2O systems, H_2 can deeply hydrogenate CO_2 to CH_4 due to its strong reducing ability, only a small amount of CO was generated. In CO_2+H_2 system, the effect of electronic promoters on the reduction degree of the CO_2 reaction was not obvious, but the trend was the same. It also confirmed that modification of In_2O_3 with F^- (electron donors) and NH_2^+ ions (electron acceptors) effectively regulated product selectivity, where the reduction degree of the CO_2 reaction increased and decreased, respectively.

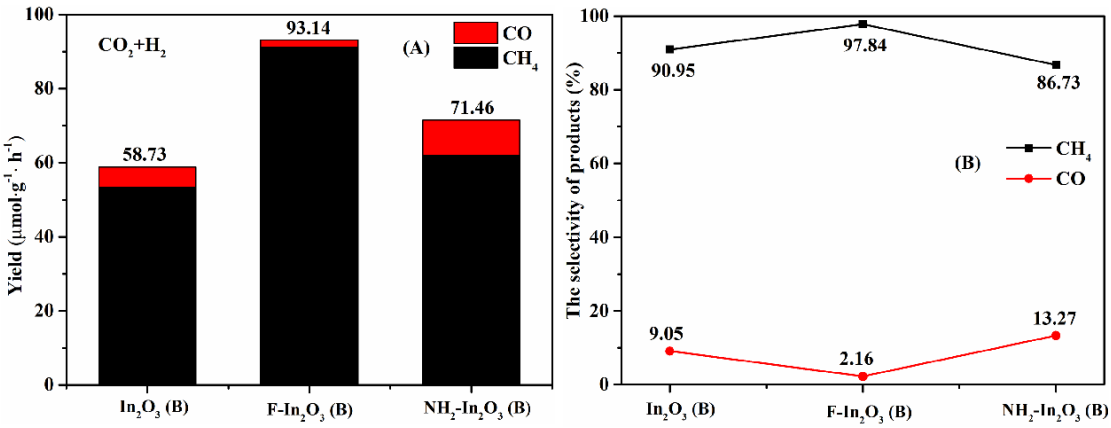

Fig. S8 Yields of photocatalytic CO_2+H_2 reaction (A) and product selectivity (B) over In_2O_3(B), F-In_2O_3(B) and NH_2-In_2O_3(B) samples under UV radiation after 1 h.

XPS Analysis

XPS survey spectra of the three samples in Fig. S9 and Table S3, the In_2O_3(B) (Fig. S9-a) reveals that the surface of the sample was composed of the elements of indium and oxygen, the C1s peak located at the binding energy of 284.8 eV was generated from the correction for specimen charging by referencing C [7]. The F-In_2O_3(B) (Fig. S9-b) and NH_2-In_2O_3(B) (Fig. S9-c) indicates the similar elements to the pure In_2O_3, but some peaks were assigned to F1s and N1s, respectively. The atomic ratio of O:In in samples have been also calculated from the XPS survey spectra to be about 1.77, 1.82 and 2.28 for In_2O_3(B), F-In_2O_3(B) and NH_2-In_2O_3(B) samples, respectively. These values are very close to results of EDS elemental mapping (Fig. 8). Notably, the three samples contain such high level oxygen elemental, it is possible that all samples were rich in surfaces oxygen vacancy defects, resulting in more the O_v and adsorbed oxygen species on the surface. At this time, the oxygen elemental detected by XPS and EDS spectrum contains a variety of oxygen species (O_{lat}, O_v and adsorbed oxygen species). Through comparative analysis, it can be found that the larger the surface oxygen vacancy concentration (Fig. 3), the higher ratio of oxygen elemental (Fig. 8 and Table S3), which was also consistent with the results of XPS-O1s spectrum. Moreover, there are scanning depth and width differences on two instruments, resulting in different results of the content of F and N elements in the two test methods (EDS and XPS spectrum).

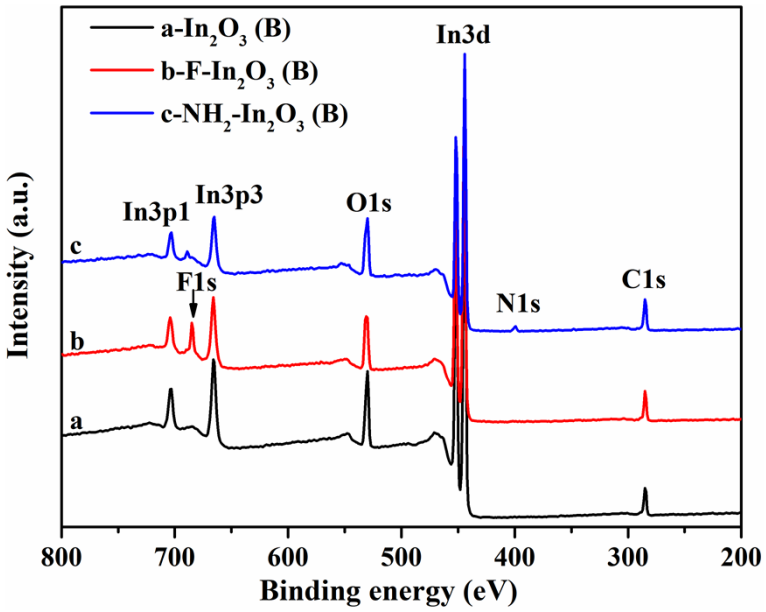

Fig. S9 XPS survey spectra of the (a) In_2O_3(B), (b) F-In_2O_3(B) and (c) NH_2-In_2O_3(B) samples.

Table S1 The calculated atomic content from the XPS survey spectra of samples.

Sample	Name	Peak BE	Area (P) CPS.eV	Area (N) TPP-2M	Atomic (%)	Atomic ratios of O/In
In_2O_3(B)	C1s	284.80	85985.71	1205.73	31.38	1.77
	In3d	444.18	1963610.08	952.39	24.79	
	O1s	529.73	290728.49	1683.69	43.83	
F-In_2O_3 (B)	C1s	284.80	83267.81	1167.61	30.19	1.82
	F1s	684.72	122538.37	566.70	14.65	
	In3d	444.54	1557622.58	755.67	19.54	
	O1s	530.65	237630.21	1377.18	35.61	
NH_2-In_2O_3(B)	C1s	284.80	97000.38	1360.18	38.61	2.28
	N1s	399.37	16748.52	151.30	4.29	
	In3d	444.03	1264510.11	613.24	17.41	
	O1s	529.65	241414.28	1398.01	39.69	

Table S2 Variation of various characteristic peaks from the O1s XPS of In_2O_3(B), F-In_2O_3(B) and NH_2-2In_2O_3(B) samples before and after adsorption.

Sample	Name	Peak BE	Area (eV)	Atomic (%)
In_2O_3 (B)-Before	O_{lat}	529.71	181377.28	60.95
	O_v	531.43	116073.57	39.05
In_2O_3 (B)-After	O_{lat}	529.76	175285.45	58.79
	O_v	531.36	122752.56	41.21
F-In_2O_3 (B)-Before	O_{lat}	529.81	98350.75	40.64
	O_v	531.66	143488.65	59.36
F-In_2O_3 (B)-After	O_{lat}	529.71	125027.44	40.50
	O_v	531.72	183455.50	59.50
NH_2-In_2O_3(B)-Before	O_{lat}	529.53	108185.34	43.90
	In-O-N	530.57	48596.34	19.73
	O_v	532.00	89496.33	36.37
NH_2-In_2O_3(B)-After	O_{lat}	529.66	104343.23	37.88
	In-O-N	530.43	61905.14	22.48
	O_v	531.97	109033.24	39.64

Table S3 Variation of various characteristic peaks from the F1s and N1s XPS of F-In_2O_3(B) and NH_2-In_2O_3(B) samples before and after adsorption.

Sample	Name	Peak BE	Area (eV)	Atomic (%)
F-In_2O_3 (B)-Before	InF_3	684.69	110392.32	95.30
	O-In-F_{lat}	688.67	5426.49	4.70
F-In_2O_3 (B)-After	InF_3	684.88	58065.32	85.11
	O-In-F_{lat}	688.61	10131.60	14.89
NH_2-In_2O_3 (B)-Before	-NH_2	399.32	13164.10	81.10
	-NH_3^+	401.04	3064.80	18.90
NH_2-In_2O_3 (B)-After	-NH_2	399.46	3741.89	50.43
	-NH_3^+	400.29	3677.03	49.57

References:

1. Z.M. Wang, H. Wang, X.X. Wang, X. Chen, Y. Yu, W.X. Dai and X.Z. Fu, *Chinese J. Catal*, 2021, **42**, 1538-1552.

2. D.M. Zhao, C.L. Dong, B. Wang, C. Chen, Y.C. Huang, Z.D. Diao, S.Z. Li, L.J. Guo and S.H. Shen, *Adv. Mater.*, 2019, **31**, 1903545.

3. H.J. Yu, R. Shi, Y.X. Zhao, T. Bian, Y.F. Zhao, C. Zhou, G.I.N. Waterhouse, L.Z. Wu, C.H. Tung and T.R. Zhang, *Adv. Mater.*, 2017, **29**, 1605148.

4. P. Makuła, M. Pacia and W. Macyk, *J. Phys. Chem. Lett.*, 2018, **9**, 6814-6817.

5. V.V.C. Lima, F.B.D. Nora, E.C. Peres, G.S. Reis, É.C. Lima, M.L.S. Oliveira and

G.L. Dotto, J Environ Eng, 2019, **7**, 103410.

6. W.W. Wang, W.Z. Yu, P.P. Du, H. Xu, Z. Jin, R. Si, C. Ma, S. Shi, C.J. Jia and C.H. Yan, ACS Catal., 2017, **7**, 1313-1329.
7. X.H. Yang, H.T. Fu, Y. Tian, Q. Xie, S.X. Xiong, D.Z. Han, H. Zhang, X.Z. An, Sens. Actuators B Chem., 2019, **296**, 126696.